Preparation and Photoelectrochemical Performance of Potassium Hexatitanate Nanofilm

QIAN Qing-hua(钱清华)[1,2], LIU Chang(刘 畅)[1], HU Yu-yan(胡煜艳)[1],
YANG Zhu-hong(杨祝红)[1], FENG Xin(冯 新)[1], LU Xiao-hua(陆小华)[1]

(*1. College of Chemistry and Chemical Engineering, Nanjing University of Technology, Nanjing, Jiangsu 210009, China; 2. Lianyungang Technical College, Lianyungang, Jiangsu 222006, China*)

Abstract: Nanostructured $K_2Ti_6O_{13}$ film photoelectrode produced *in situ* was prepared on indium–tin oxide (ITO) glass substrate by a sol–gel process and characterized by thermogravimetry (TG) and differential scanning calorimetry (DSC), X-ray diffraction (XRD), atomic force microscopy (AFM), UV–Visible diffuse reflectance and Raman spectrometry. The photoelectrochemical performance of $K_2Ti_6O_{13}$ film was assessed by electrochemical method. The analytical results showed that the $K_2Ti_6O_{13}$ film had a strong and wide absorption in the ultraviolet and visible light range. The band gap energy (E_g) of the film shifted from 3.45 eV (bulk) to 3.05 eV (film). The flat-band potential (E_{fb}) of $K_2Ti_6O_{13}$ film was −0.67 V [vs. saturated calomel electrode (SCE)]. The transport of photogenerated electrons and holes was better in $K_2Ti_6O_{13}$ film electrode than that in TiO_2 film electrode. The photoelectrochemical response of $K_2Ti_6O_{13}$ photoelectrode was increased in electrolyte solution with KOH, compared with that in the solution without KOH. The adsorption of OH^- on the nanofilm acted as the surface activity center. The mechanism of photolysis was analyzed in terms of photoelectrochemical behavior.

Key words: potassium hexatitanate film; sol–gel process; atomic force microscopy; photoelectrochemical performance
CLC No.: 0643 **Document Code:** A **Article ID:** 1009−606X(2007)05−1022−07

1 INTRODUCTION

The process of converting light into electric power or chemical fuels has been intensively studied by researchers since Edmond Becquerel discovered the photoelectric effect[1]. Photoelectrolysis of water with the use of semiconductor photoelectrodes is a non-polluting, wasteless and renewable method for production of energy. The behavior of semiconductor electrodes in photoelectrochemical response can be correlated with the photocatalytic activity of semiconductor. Photocatalysis has also been actively studied[2]. Especially, the research of photocatalysts has been focused on the treatment of environmental pollutants by strong oxidizing power of hydroxyl radical produced by light exposure.

$K_2Ti_6O_{13}$ is a tunnel mixed metal oxide ($K_2O{\cdot}6TiO_2$) with semiconductor behavior, and has thermal durability, chemical resistivity, dispersibility and high photocatalystic activity[3−8]. It was found that its photocatalytic activity is higher than those of layered mixed oxides and other tunnel mixed oxides in the photocatalytic production of hydrogen from water[9]. However, $K_2Ti_6O_{13}$ has a wide band gap of about 3.45 eV. Although many investigations were carried out in order to enhance photocatalytic activity[7,8], the band gap had not been altered. The photoelectrochemical performance of $K_2Ti_6O_{13}$ was not reported yet.

The photoelectrochemical measurement of a semiconductor is mainly used to evaluate its photocatalytic activity, and thin film electrodes are necessary for such investigations. Many methods have been developed to prepare films. Among them, sol–gel route has many advantages such as easy control of the composition, excellent homogeneity on the molecular, even atom level, the ability to coat large area of high quality thin film and low crystallization temperature[10].

Although the films can be prepared by powder coating, the method may result in many defects such as coarse surface and infirm force between the films and substrate. In this work, $K_2Ti_6O_{13}$ film electrode produced *in situ* was prepared by a sol–gel method. The film was characterized by thermogravimetry (TG) and differential scanning calorimetry (DSC), X-ray diffraction (XRD), atomic force microscopy (AFM), UV–Visible diffuse reflectance and Raman spectrometry. The photoelectrochemical behavior of the film was analyzed and the photocatalytic mechanism for H_2O photolysis in alkaline solution was analyzed. Similar measurements were carried out on TiO_2 film

Received date: 2006−12−31; **Accepted date:** 2007−03−20
Foundation item: Supported by the National Natural Science Foundation of China (No. 20246002; 20236010); National High Technology Research and Development Program of China (No. 2003CB615700); The Key Science Foundation of Jiangsu Province (No. BK 2004215)
Biography: QIAN Qing-hua (1965–), female, native of Lianyungang City, Jiangsu Province, Ph.D., associate professor, research in thin nanofilm materials and materials chemistry; LU Xiao-hua, Corresponding author, Tel: 025-83067183, Fax: 025-83588063, E-mail: xhlu@njut.edu.cn.

with the same thickness for comparison.

2 EXPERIMENTAL

2.1 Materials and Reagents

Tetrabutyl titanate [Ti(n-OC_4H_9)$_4$, Shanghai No.3 Reagents Co., 98.0% purity, China], indium−tin oxide (ITO) glass (~15 Ω/cm^2, Shenzhen Csgholding Co., Ltd., China), potassium acetate (CH_3COOK, Shanghai Chemical Reagents Co., China Medicine Group, 92% purity), acetylacetone ($CH_3COCH_2COCH_3$, Shanghai Chemical Reagents Co., China Medicine Group, 98.5% purity), 2-methoxyethanol ($CH_3OCH_2CH_2OH$, Shanghai No.1 Lingfeng Chemical Co., 99% purity). All reagents with analytical grade were used without further purification.

2.2 Preparation of TiO_2 Film

TiO_2 film was prepared by Ti(n-OC_4H_9)$_4$ hydrolysis in alcoholic solution and dip-coating method. Ti(n-OC_4H_9)$_4$ was added into anhydrous ethanol under stirring. The pH value of the solution was adjusted by adding HNO_3. A mixture of deionized water and acetylacetone was added into the former Ti(n-OC_4H_9)$_4$ solution dropwise. The chemical composition of the alkoxide solution was Ti(n-OC_4H_9)$_4$:C_2H_5OH:H_2O:$CH_3COCH_2COCH_3$=1.0:26.4:2.0:0.5 in molar ratio. Prior to the film deposition, ITO glass was treated by acetone and alcohol, and dried thereafter. TiO_2 film was deposited at a rate of 35 mm/min, followed by dehydration at 100℃for 10 min. The deposition and heat-treatment cycle was repeated 6 times in order to prepare thick films. Finally, the film was heated up to 500℃ at a heating rate of 3℃/min and kept for 90 min.

2.3 Preparation of $K_2Ti_6O_{13}$ Film

Acetylacetone and acetic acid were used as chelating agent and solvent, respectively. 2-Methoxyethanol was used as diluting agent to get crack-free films. Firstly, potassium acetate was dissolved in acetic acid. A stoichiometric amount of Ti(n-OC_4H_9)$_4$ was mixed with acetylacetone, followed by the addition of acetate solution with continuous stirring dropwise. A yellow homogeneous sol formed after stirring for 2 h. The molar ratio of components in sol was set as Ti(n-OC_4H_9)$_4$:CH_3COOK:CH_3COOH:$CH_3COCH_2COCH_3$=3.0:1.0:5.0:0.5. The sol was heated at 70℃ for formation of gel for TG–DSC analysis.

The clear sol was diluted with 2-methoxyethanol to adjust the viscosity and surface tension. The film was coated onto ITO glass by dip-coating. Firstly, the cleaned substrate was dipped into the prepared sol and withdrawn at a regular rate of 35 mm/min. Then, the wet film was preheated on a hot plate at 350℃ for 10 min. The deposition and heat-treatment cycle was repeated 6 times. The coating was sintered at 600℃ for 2 h. Calcination was performed in a muffle furnace with a heating rate of 5℃/min.

2.4 Characterization

Thermal analysis (TG–DSC, Model SDT 2960, TA Instruments, New Castle, UK) was performed on the dried gel with a heating rate of 20℃/min from 38℃ up to 1000℃ in nitrogen gas flow. X-ray diffraction patterns were obtained by using a D8 advance (Bruker AXS, Karlsruhe, Germany). Cu, $K\alpha$ radiation with a nickel filter and a zero-background sample cell were used, operating at 40 kV and 20 mA. All samples were measured in a continuous scanning mode in a range of 5^o~60^o (2θ) with a scanning rate of 0.05^o/s. Morphology and surface microstructure of film were characterized by AFM (AutoCP-Reaserch, PSI, USA). Raman spectra were collected using a JY Horiba LabRam HR800 microRaman spectrograph at room temperature. The thickness of film was measured with scanning electron microscope (SEM, Model JSM-6300, JEOL, Japan). The chemical composition of film was determined with energy dispersion X-ray analysis (EDXA) instrument equipped with an SEM. UV−Visible absorption spectrometer were obtained by using spectrophotometer (UV2401PC, Shimadzu, Japan).

2.5 Electrochemical Measurement

All electrochemical experiments were performed using an EG&G PARC Versastat Electrochemical System at room temperature. A 20 mL electrochemical cell was filled with saturated calomel electrode (SCE) as reference electrode, platinum sheet as auxiliary electrode and $K_2Ti_6O_{13}$ film/ITO or TiO_2 film/ITO as working electrode. 0.1 mol/L Na_2SO_4 solution was used as the supporting electrolyte in the electrochemical measurement. The working electrode with a test surface of 1.0 cm^2 was used for all experiments. An 8 W middle pressure mercury lamp with a wavelength centered at 254 nm was used as an illuminant. The intensity of UV light was kept 2.5 mW/cm^2 in all experiments.

3 RESULTS AND DISCUSSION

3.1 TG–DSC Analysis

Figure 1 shows the TG–DSC spectra for Ti(n-OC_4H_9)$_4$–CH_3COOK gel. The spectra can be divided into three weight loss steps. The first weight loss (about 10%) at T<230℃ is due to the volatilization of free water and solvent. The second one (about 31.3%) in 230~400℃ is quick, due to the partial decomposition

of organic substances and the reaction between Ti(n-OC_4H_9)$_4$ and CH_3COOK, corresponding to a broad exothermic peak centered at 300 ℃ on the DSC trace. The third one of 1.3%(ω) loss in the range 400~519 ℃ is relatively slow and steady, ending with a long step on the TG trace, which illustrates that organic solvents have been completely volatilized, but the reaction still continues. The TG trace becomes horizontal when T>519 ℃, there is no weight loss, showing that amorphous $K_2Ti_6O_{13}$ converts to crystals at temperatures higher than 519 ℃. The peak on the DSC trace at 300 ℃ is small and there is no peak at T>400 ℃, indicating that the intensities of reaction and phase change are weak.

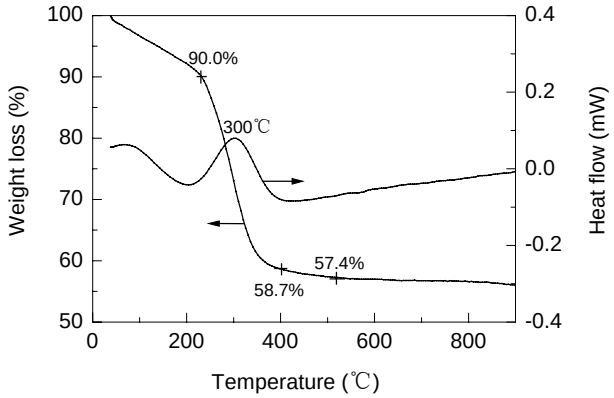

Fig.1 TG–DSC spectra of Ti(n-OC_4H_9)$_4$–CH_3COOK gel

3.2 X-ray Diffraction Results

Figure 2 shows the X-ray diffraction patterns of CH_3COOK–Ti(n-OC_4H_9)$_4$ sol–gel films sintered at different temperatures. There is only one peak with 2θ=5.9° at 100 ℃, which is the characteristic peak of potassium polyacetate. Therefore, there is no reaction occurring at 100 ℃. However, the diffraction peak of potassium polyacetate disappears completely when the sample is heated at 300 ℃. This implies that the initial reaction temperature is lower than 300 ℃. It agrees with the result of TG–DSC analysis. From thermodynamic calculations[11], the lowest temperature of reaction between TiO_2·nH_2O and K_2CO_3 is 300 ℃ during the solid state reaction process, and the improvement of reaction activity and lower reaction temperature are attributed to the presence of a nano-scale mixing state between TiO_2·nH_2O and K_2CO_3[12]. The sol–gel method also follows a soft chemistry mechanism and therefore has lowered the initial reaction temperature, compared with that of solid state reaction.

In addition, all the samples annealed from 300 ℃ to 500 ℃ are amorphous, and the characteristic peaks of $K_2Ti_6O_{13}$ appear when the films are heated at 600 ℃. The broadening of the strongest XRD peak of $K_2Ti_6O_{13}$

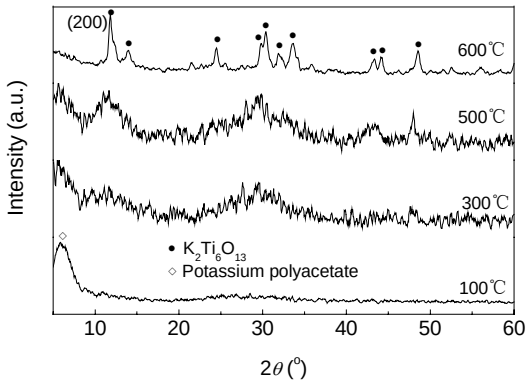

Fig.2 XRD patterns of films heated at different temperatures for 2 h

diffraction pattern at 600 ℃ indicates the formation of $K_2Ti_6O_{13}$ nanoclusters. The crystal size derived from the (200) peak of $K_2Ti_6O_{13}$ with the Scherer equation is ca. 15 nm at this temperature. This temperature is also lower than that of solid state reaction[13]. The nanocrystallites can not only enhance the photoactivity but also reduce the roughness of the films, being favorable to surface modification. Therefore, 600 ℃ is selected as the optimum temperature of the preparation of $K_2Ti_6O_{13}$ film photoelectrode.

3.3 Raman Spectrum

The crystalline structure of $K_2Ti_6O_{13}$ consists of six TiO_6 octahedra, the octahedra are joined by sharing edges. The formation of $K_2Ti_6O_{13}$ involves the rearrangement of the TiO_6 octahedra units. K^+ ions are inserted into the space between TiO_6 octahedra (Fig.3). Ti—O—K bonds are formed with some of Ti—O bonds broken, while the other Ti—O bonds would be reserved. Fig.4 shows the Raman spectrum of $K_2Ti_6O_{13}$ film heated at 600 ℃, the peaks below 510 cm^{-1} can be attributed to the K—O—Ti stretching vibration, the peak at about 655 cm^{-1} should be assigned to the Ti—O—Ti stretch in edge-shared TiO_6, the peak near 858 cm^{-1} was reported for a short Ti—O stretching

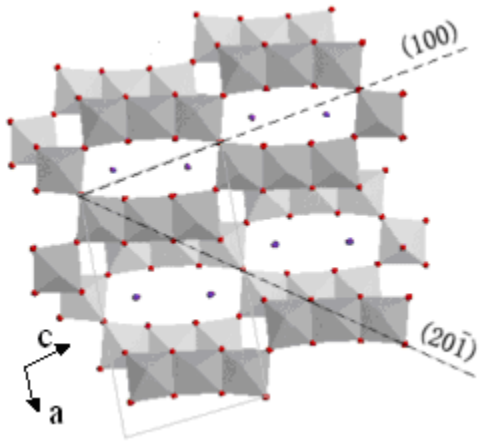

Fig.3 Idealized representation of crystal structure of $K_2Ti_6O_{13}$

vibration in distorted TiO_6, the weak peak at 399 cm^{-1} is characteristic of the K—O—Ti containing short Ti—O bonds[14]. This spectrum of $K_2Ti_6O_{13}$ film is basically similar to that of the bulk $K_2Ti_6O_{13}$[15].

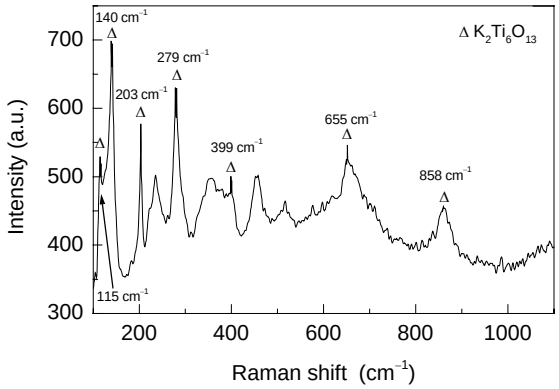

Fig.4 Raman spectrum of $K_2Ti_6O_{13}$ film heated at 600 ℃ for 2 h

The EDX spectrum studies performed on the $K_2Ti_6O_{13}$ film exhibited the presence of K and Ti with a molar ratio close to 1:3 (Fig.5), which is also consistent with $K_2Ti_6O_{13}$. The element analyses of the film from the EDX studies revealed that the film contains carbon.

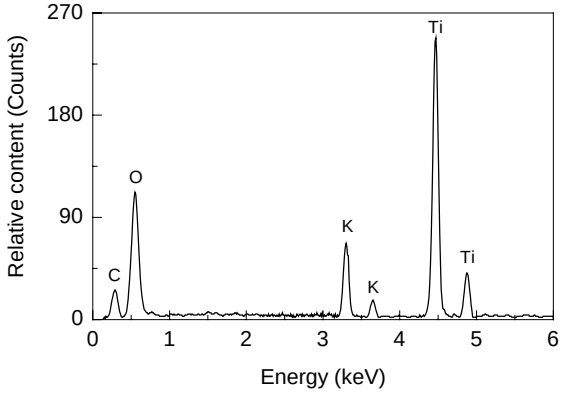

Fig.5 EDX spectrum analyzed on $K_2Ti_6O_{13}$ film

From the analytical results of TG–DSC, XRD and Raman spectra, it can be deduced that the whole reaction process for preparing $K_2Ti_6O_{13}$ from CH_3COOK and Ti(n-OC_4H_9)$_4$ is expressed as follows:

$$2CH_3COOK+6Ti(OC_4H_9)\xrightarrow{300^\circ C}$$

$$\text{Amorphous}\xrightarrow{519^\circ C}K_2Ti_6O_{13}(\text{nano crystals}).$$

3.4 Surface Structure of $K_2Ti_6O_{13}$ Film

Two-dimensional AFM image [Fig.6(a)] and cross section image [Fig.6(b) line A–A′] of $K_2Ti_6O_{13}$ film heated at 600 ℃ are displayed in Fig.6. The thickness of the film is 300 nm. The films consist of flat particles with the sizes ranging typically from 80 to 180 nm. The surface is dense, uniform and smooth. There are some nanometer interspaces in the films. Compared with the XRD data, the particles on the film exist in aggregation of nanocrystals because each layer was preheated one time at 350 ℃ for 10 min during the film deposition process. The root mean square (RMS) roughness of the films based on the measurement of an area of 2 μm×2 μm in AFM images is only 6.4 nm.

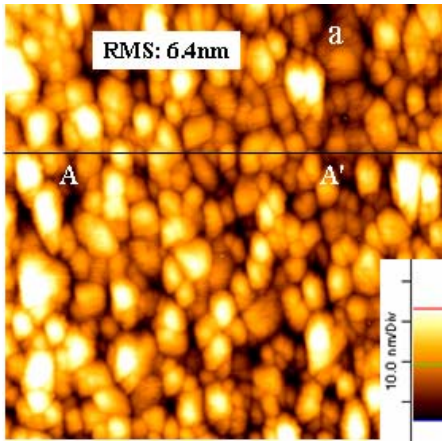

(a) 2 μm×2 μm 2D AFM image

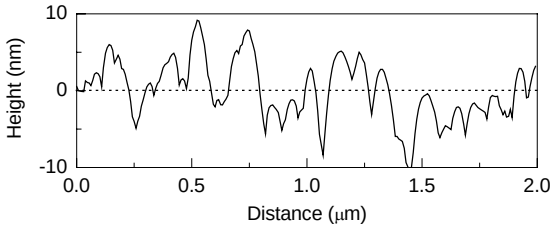

(b) Cross section image of line A–A′ in (a)

Fig.6 The analysis of surface structure of $K_2Ti_6O_{13}$ film

3.5 UV–Vis Spectra of the Films

Both wetting films and sintered films are compact and transparent on glass. Fig.7 shows the typical UV–Visible absorption spectra of $K_2Ti_6O_{13}$ and TiO_2 films. According to the visual observations the transparent nanofilms have fine and quite homogeneous structure and show interference colors in visible light. It is evident that the absorption of TiO_2 film is lower than that of $K_2Ti_6O_{13}$ film in the wavelength range of 300~700 nm. The TiO_2 film almost has no absorption above 400 nm. The band gap energy (E_g) of films can be estimated from the absorption coefficient by fitting the data to the correlation:

$$(ah_v)^{1/2}=B(h_v-E_g), \quad (1)$$

where α is the absorption coefficient, $\alpha=A/d$, A absorbency, d film thickness, h_v incident photon energy, and B edge width parameter[16]. The values of band gap energy E_g are 3.05 and 3.22 eV for $K_2Ti_6O_{13}$ film and

TiO_2 film, respectively. The λ_{onset} of $K_2Ti_6O_{13}$ film is seen to be different from those of the TiO_2 film (about 400 nm, corresponding to a band gap of 3.22 eV) and bulk $K_2Ti_6O_{13}$ sample (about 370 nm, corresponding to a band gap of 3.45 eV)[3]. Compared with a bulk $K_2Ti_6O_{13}$ sample, the spectrum of the $K_2Ti_6O_{13}$ film shows strong and wide absorption in the ultraviolet and visible region, which can be ascribed to the non-uniformity of defects and size distribution of the $K_2Ti_6O_{13}$ film.

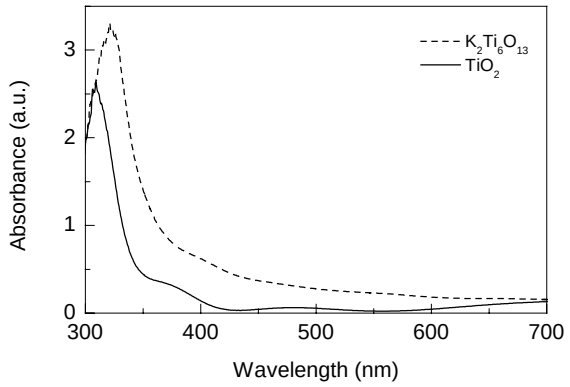

Fig.7 UV−Visible diffuse reflectance of $K_2Ti_6O_{13}$ and TiO_2 films

3.6 Photoelectrochemical Performance

Transient photocurrent variations, open circuit potentials and voltammogram curves of $K_2Ti_6O_{13}$/ITO and TiO_2/ITO films are shown in Fig.8. Upon absorption of light by $K_2O{\cdot}6TiO_2$ semiconductor, electrons are promoted to the conduction band (e_{cb}^-), and holes are left in the valence band (h_{vb}^+):

$$K_2O\cdot 6TiO_2 \xrightarrow{h\nu} K_2O\cdot 6TiO_2(e^-, h^+). \quad (2)$$

They are so spatially close to each other as to be called electron–hole pairs, and easily recombined. At bulk semiconductor and electrolyte interface, the inner electric field separates the pairs spatially, prolonging their lifetime. In water photolysis with semiconductive photocatalysts, electrons and holes produced under the illumination of light with energy higher than the band gap reduce and oxidize H_2O to produce H_2 and O_2, respectively.

Figure 8(a) shows that the photocurrent of film electrodes reaches saturated state quickly when light is turned on due to the production of photogenerated carriers. Eventually, steady states are attained with approximately unchanging photocurrent values, owing to the balancing rate between creation and depletion of photogenerated carriers[17]. The photocurrent of $K_2Ti_6O_{13}$ film electrodes is also higher and stabler than that of TiO_2 electrode, which demonstrates that the charges of holes and electrons in $K_2Ti_6O_{13}$ film have been effectively separated. However, the photocurrent of TiO_2 electrode drops steadily as time proceeds when it reaches saturated state. Gerischer et al.[18] reported that O_2 acted as the electron acceptor and could produce O_2^- when it reacted with e^- during photoelectrochemical reactions. TiO_2 shows a sufficiently fast O_2 reduction rate[19], resulting in the photocurrent of TiO_2 electrode dropping slowly. While $K_2Ti_6O_{13}$ film electrodes possess a stable photocurrent, which indicates that the transport of photogenerated electrons and holes is good in $K_2Ti_6O_{13}$ film electrode.

Figure 8(b) shows that the open circuit potentials of $K_2Ti_6O_{13}$ and TiO_2 film electrodes (TiO_2 1.35 V, $K_2Ti_6O_{13}$ 1.52 V) decrease rapidly down to lower values as a result of the sudden creation of electron–hole pairs in the films when the films are illuminated by UV light. The open circuit potential tendes to stabilize and then attains a plateau that could be attributed to further accumulation of photogenerated electrons in the conduction band and formation of new surface species (Ti^{4+}–O_2^{2-})[17]. The open circuit potential of $K_2Ti_6O_{13}$ decreases sharply when the light is turned on and then increases slowly when the light is turned off. This result indicates that the recombination rate of photogenerated

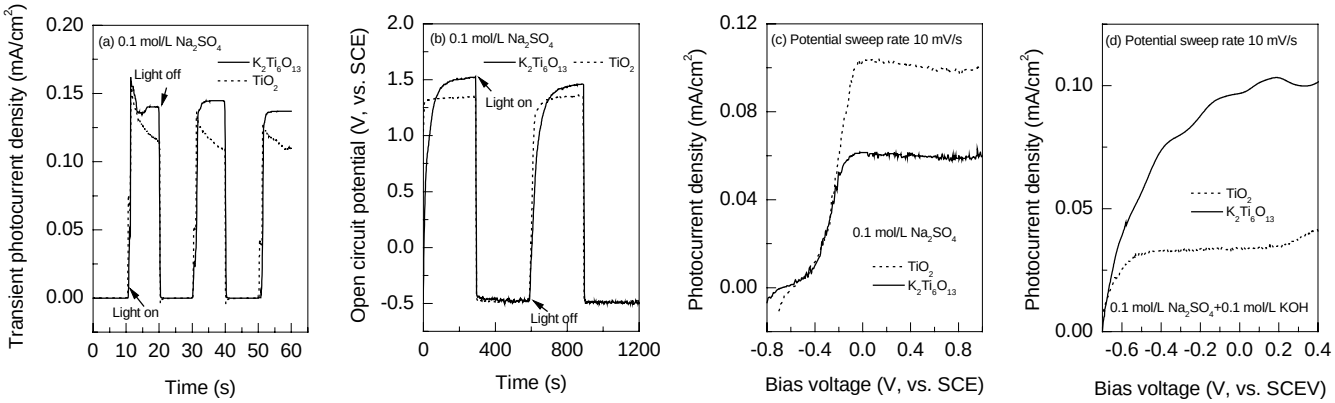

Fig.8 Photoelectrochemical performance of $K_2Ti_6O_{13}$/ITO and TiO_2/ITO films

electron–hole is slow for $K_2Ti_6O_{13}$ films. The electrode remains charged even after the lamp is switched off.

It can be seen from Fig.8(c) that the flat-band potential (E_{fb}) of $K_2Ti_6O_{13}$ and TiO_2 films is –0.67 and –0.51 V, respectively. The E_{fb} of $K_2Ti_6O_{13}$ film is lower than that of TiO_2 film, illustrating that the reductivity of $K_2Ti_6O_{13}$ film is better than that of TiO_2 film. Fig.8(d) shows the typical voltammograms of $K_2Ti_6O_{13}$ film electrodes in the solution of 0.1 mol/L Na_2SO_4 and 0.1 mol/L KOH ($V_{Na_2SO_4(aqu.)}$:$V_{KOH(aqu.)}$=1:1). Higher photocurrent is observed in the solution with KOH than that in the solution without KOH [Fig.8(c)] when the $K_2Ti_6O_{13}$ film is illuminated. The photocurrent of $K_2Ti_6O_{13}$ photoelectrode increases in the solution of 0.1 mol/L Na_2SO_4 and 0.1 mol/L KOH, compared with that in 0.1 mol/L Na_2SO_4 solution, and the photocurrent of $K_2Ti_6O_{13}$ photoelectrode is higher than that of TiO_2 film, indicating that photolysis of H_2O is easier in alkaline electrolyte solution than that in Na_2SO_4 solution and the performance of $K_2Ti_6O_{13}$ is better than TiO_2 in alkaline electrolyte solution.

A scheme of the mechanism of photolysis of H_2O in the presence of KOH is illustrated in Fig.9. The figure shows the charge transfer mechanism and possible electrochemical reactions involving produced electrons and holes in the semiconductor film under illumination. The electron–hole separation occurs serially on the surface of $K_2Ti_6O_{13}$ film under illumination, which produces higher photocurrent, as seen in Fig.8(d). The photocurrent of $K_2Ti_6O_{13}$ film increases largely in the range of 0.5~1.5 V due to the formation and oxidation of new surface species (Ti^{4+}–O_2^{2-}) adsorbed on the surface of the film[18]. Almost all of the produced electrons and holes will immediately reach the film surface or edge because their thickness is very thin, bulk recombination can be neglected. OH^- in alkaline solution will easily adsorb on the film surface for the hydrophilic property and be oxidized by the hole ($K_2O{\cdot}TiO_2^+$) reaching the surface, subsequently generating highly reactive ·OH radicals in the solution and further promoting the production of the electron–hole pairs. Meanwhile the surface electron will bring about the H_2O reduction to produce H_2. The whole reaction process is expressed as follows[18]:

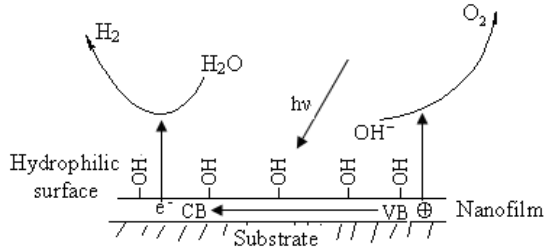

Fig.9 A scheme of the mechanism of water photolysis in 0.1 mol/L Na_2SO_4+0.1 mol/L KOH solution

$$K_2O{\cdot}6TiO_2^+ + OH^- \longrightarrow K_2O{\cdot}6TiO_2 + {\cdot}OH, \quad (3)$$

·OH can be further separated into hydrated oxygen ions and hydrated hydrogen ions:

$$\cdot OH \rightarrow O_{aq}^- + H_{aq}^+, \quad (4)$$

$$K_2O{\cdot}6TiO_2^+ + O_{aq}^- \rightarrow K_2O{\cdot}6TiO_2 + O_{ads}, \quad (5)$$

$$2O_{ads} \rightarrow O_2\uparrow. \quad (6)$$

The photoelectrons subsequently pass into the external circuit and to the auxiliary electrode, where the reduction of water takes place. On Pt cathode, the electrons from photoanode can be combined with hydrated hydrogen ions:

$$H_{aq}^+ + e^- \rightarrow H_{ads}\ ,\ 2H_{ads} \rightarrow H_2\uparrow\ . \quad (7)$$

The presence of the adsorbed OH^- will relatively reduce the recombination rate between the surface holes and electrons because the concentration of holes on the surface decreases as a result of rapid transfer to OH^- for its higher tendency to capture holes. Consequently, the presence of OH^- promotes H_2 evolution under illumination due to the decrease in the surface recombination rate of the photogenerated electrons and holes.

4 CONCLUSIONS

(1) Nanostructured $K_2Ti_6O_{13}$ film was prepared on glass substrate via a sol–gel method by controlling the molar ratio of CH_3COOK to Ti(n-OC_4H_9)$_4$ in sol. The nanofilm is smooth, compact and transparent, and had fine and quite homogeneous structure. The starting reaction temperature of this system is lower than 300℃ and $K_2Ti_6O_{13}$ nanocrystals form at 600℃, with the original grain size about 15 nm.

(2) The photocurrent of $K_2Ti_6O_{13}$ film electrode is more stable than that of TiO_2 film electrode. The photocurrent of $K_2Ti_6O_{13}$ photoelectrode is increased in alkaline solution, compared with that in 0.1 mol/L Na_2SO_4 solution.

(3) The band gap energy (E_g) of the film is 3.05 eV. The flat-band potential (E_{fb}) of $K_2Ti_6O_{13}$ is –0.67 V [vs. saturated calomel electrode (SCE)]. The reduction of $K_2Ti_6O_{13}$ film is stronger than that of TiO_2 film. Both the separation ability of photogenerated electron–hole

pairs and the photoelectrochemical response of $K_2Ti_6O_{13}$ photoelectrode are better as the band gap energy becomes narrow.

REFERENCES:

[1] Grätzel M. Photoelectrochemical Cells [J]. Nature, 2001, 414: 338–344.

[2] Sun X L, Zhang G L, Zhang F B. Gas-phase Photocatalytic Activity of TiO_2 Doped with Ag and Ni [J]. Chin. J. Process Eng., 2005, 5(5): 576–579 (in Chinese).

[3] Du G H, Chen Q, Han P D. Potassium Titanate Nanowires: Structure, Growth, and Optical Properties [J]. Phys. Rev. B, 2003, 67: 035323-1–035323-7.

[4] Chatterjee A, Hayashi H, Iwasaki T. First Principle Study to Correlate Location and Activity of Ruthenium Oxide Incorporated in Alkali-metal Hexatitanates [J]. J. Phys. Chem. B, 2001, 105: 3463–3469.

[5] Feng X, LU J Z, Lu X H. Applications of Potassium Titanate Whiskers in Composite Materials [J]. Acta Mater. Comp. Sinica, 1999, 16: 1–6.

[6] Hakuta Y, Hayashi H, Arai K. Hydrothermal Synthesis of Photocatalyst Potassium Hexatitanate Nanowires under Supercritical Conditions [J]. J. Mater. Sci., 2004, 39: 4977–4980.

[7] Guan G Q, Kida T, Harada T, et al. Photoreduction of Carbon Dioxide with Water over $K_2Ti_6O_{13}$ Photocatalyst Combined with Cu/ZnO Catalyst under Concentrated Sunlight [J]. Appl. Catal. A: Gen., 2003, 249: 11–18.

[8] Yahya R B, Hayashi H, Nagase T, et al. Hydrothermal Synthesis of Potassium Hexatitanates under Subcritical and Supercritical Water Conditions and Its Application in Photocatalysis [J]. Chem. Mater., 2001, 13: 842–847.

[9] Shangguan W F, Yoshida A. Influence of Catalyst Structure and Modification on the Photocatalytic Production of Hydrogen from Water on Mixed Metal Oxides [J]. Int. J. Hydrogen Energy, 1999, 24: 425–431.

[10] Hench L L, West J K. The Sol–Gel Process [J]. Chem. Rev., 1990, 90(1): 33–72.

[11] Bao N Z, Feng X, Lu X H. Low-temperature Controllable Calcination Synthesis of Potassium Dititanate [J]. AIChE J., 2004, 50: 1568–1577.

[12] Yu L, He M, Liu C, et al. Nano-scale Mixing of $TiO_2{\cdot}nH_2O$ and Potassium Carbonate [J]. Mater. Chem. Phys., 2005, 93: 342–347.

[13] Liu C, Lu X H, Yu G, et al. Role of an Intermediate Phase in Solid State Reaction of Hydrous Titanium Oxide with Potassium Carbonate [J]. Mater. Chem. Phys., 2005, 94: 401–407.

[14] Meng X D, Wang D Z, Liu J H, et al. Effects of Titania Different Phases on the Microstructure and Properties of $K_2Ti_6O_{13}$ Nanowires [J]. Solid State Commun., 2006, 137: 146–149.

[15] Bamberger C E, Begun G M, MacDougall C S. Raman Spectroscopy of Potassium Titanates: Their Synthesis, Hydrolytic Reactions, and Thermal Stability [J]. Appl. Spectrosc., 1990, 44: 30–37.

[16] Wang B L, Hu L L. Optical and Surface Properties of Hybrid TiO_2/Ormosil Planar Waveguide Prepared by the Sol–Gel Process [J]. Ceram. Int., 2006, 32: 7–12.

[17] Beermann N, Boschloo G, Hagfeldt A. Trapping of Electrons in Nanostructured TiO_2 Studied by Photocurrent Transients [J]. J. Photochem. Photobiol. A: Chem., 2002, 152: 213–218.

[18] Gerischer H, Heller A. The Role of Oxygen in Photooxidation of Organic Molecules on Semiconductor Particles [J]. J. Phys. Chem., 1991, 95: 5261–5267.

[19] Byrne J A, Davidson A, Dunlop P S M, et al. Water Treatment Using Nano-crystalline TiO_2 Electrodes [J]. J. Photochem. Photobiol. A: Chem., 2002, 148: 365–374.